In matrix form for a binary system

$$\begin{bmatrix} \lambda m_{1,1} - 1 & \lambda m_{1,2} \\ \lambda m_{2,1} & \lambda m_{2,2} - 1 \end{bmatrix} \begin{bmatrix} dC_1 \\ dC_2 \end{bmatrix} = \begin{bmatrix} 0 \\ 0 \end{bmatrix} \tag{24}$$

The characteristic equation giving the eigenvalues for Eq. 24 is

$$(\lambda m_{1,1} - 1)(\lambda m_{2,2} - 1) - m_{1,2}\, m_{2,1}\, \lambda^2 = 0$$

which yields

$$\lambda = \frac{m_{1,1} \pm ((m_{1,1} - m_{2,2})^2 + 4 m_{1,2}\, m_{2,1})^{1/2}}{2(m_{1,1}\, m_{2,2} - m_{1,2}\, m_{2,1})} \tag{25}$$

and the eigenvectors are

$$\frac{dC_1}{dC_2} = \frac{\lambda m_{1,2}}{1 - \lambda m_{1,1}} \tag{26}$$

In order to construct a composition path in the $(C_1 - C_2)$-plane, one chooses a composition near the boundary, then evaluates Eqs. 25 and 26 from the definitions of the $m_{i,j}$ and the relations

$$C_{i,t} = \overline{C}_i + C_i$$

$$\overline{C}_i = K_i\, C_{i,d}$$

$$\phi \sum C_{i,d} = \left[\frac{(\Pi \phi C_i^*)^\theta}{\sum x_i \left(\prod_{i \neq j} \phi C_j^* \right)^\theta} \right]^{1/\theta}$$

$$\frac{C_{1,m}}{C_{2,m}} = \frac{C_{1,d}}{C_{2,d}} \left(\frac{C_2^*}{C_1^*} \right)^\theta$$

This system is highly nonlinear, so that the values of the $m_{i,j}$ must be evaluated numerically (e.g., by Newton's method) and Eq. 26 must be integrated numerically for each eigenvalue, as, for example, in this work, the Runge-Kutta-Gill algorithm was used.

As noted in the body of the paper, when the eigenvelocities along a composition path decrease in the direction of flow, as, for example, in Figures 4a and 5a which correspond to cases 2 and 3, the composition paths constructed as above no longer describe the system behavior. This is because the shock wave that arises in the column presents a discontinuity across which Eq. 6 no longer applies. The wave velocity and composition of the intermediate zone can no longer be determined from the composition path grid. However, a simple mass balance across the shock front yields the relation

$$V_{c_i} = \frac{V}{1 + \dfrac{\Delta \overline{C}_i}{\Delta C_i}} \tag{27}$$

for a coherent shock we still require that

$$V_{c_i} = V_{c_2}$$

Equation 27 must be solved by trial and error to obtain $\Lambda = V_{c_i}/V$ and the composition of the intermediate zone. In case 3, Figure 5 a1, it can be seen that composition A, the intermediate composition arising between the injected composition I and the original composition 0, is only slightly off the composition path through I. In this case, the composition obtained from constructing the composition route without accounting for shock formation is only slightly in error. However, in figure 4 a1, the composition B obtained from Eq. 27 differs considerably from the composition which would be obtained by following the composition paths. This is because of the presence of the CMC discontinuity across the composition path.

Dynamic Contact Angles

E. B. GUTOFF
and C. E. KENDRICK
Polaroid Corp. Waltham, MA 02254

The dynamic contact angles of various liquids on a gelatin-subbed polyester tape were investigated by plunging a tape into a pool of liquid, in the manner of Perry and of Burley and Kennedy. The effect of the upper fluid was studied by replacing the air normally present by immiscible oils. A fair correlation was found at the point of air entrainment, relating the capillary number, $\mu V/\sigma$, to a physical properties number, $g\mu^4/\rho\sigma^3$. A dimensional correlation, relating the air entrainment velocity to the viscosity to the −0.67 power, was even better. At various velocities, the dynamic contact angle (or the dynamic contact angle minus the static angle) could be related to the capillary number, the physical properties number, and to density and viscosity ratios. Again, the dimensional correlations were better than the dimensionless ones, perhaps caused by an omission of a significant dimensionless group due to our inability to choose a suitable characteristic length.

With any one system, the data could be expressed as $\theta = kN_{Ca}^b$ above some minimum velocity, or, covering all velocities, as $(\theta - \theta_s) = kN_{Ca}^b$. With air as the upper fluid, all the data at one angle lie within one decade, with capillary numbers at air entrainment in the range of 0.6–1.3.

SCOPE

In most coating operations the coating solution forms a dynamic contact line with the moving base, with air as the third phase. The maximum coating speed is often limited to that base velocity at which air is entrained by the moving base into the coating solution. At that point the dynamic contact angle reaches 180°. This study extends the work of Burley and Kennedy (1976b, 1978) and Perry (1967) on the effect of fluid properties and base velocity on dynamic contact angles, by plunging a gelatin-subbed polyester tape into various liquids. The effect of the third phase, usually air, was studied by replacing the air with immiscible oils.

As there is no readily accessible characteristic length, only two dimensionless ratios of forces can be involved. By dimensional analysis the dynamic contact angle should be correlated with the capillary number, $N_{Ca} = \mu V/\sigma$, a physical properties number, $N_{pp} = g\mu^4/\rho\sigma^3$, and ratios of the physical properties of two fluids, and perhaps to the static contact angle.

ISSN-0001-1541-82-4437-0459-$2.00.

CONCLUSIONS AND SIGNIFICANCE

The dynamic contact angles of any one liquid on a gelatin-subbed polyester base is simply related to the capillary number by $\theta = kN_{Ca}^{b}$. To extend this to the very low velocity region where the dynamic angle approaches the static contact angle, the static contact angle can be introduced as $(\theta - \theta_s) = kN_{Ca}^{b}$. With air as the third phase all the data at one angle lie within one decade of capillary numbers, and the numbers at air entrainment are 0.6–1.3. A generalized correlation, with a low correlation coefficient squared of only 0.70, is

$$\theta = 402\, N_{Ca,b}^{0.20}\, N_{pp}^{-0.0096}(\rho_t/\rho_b)^{0.11}(\rho_b/\Delta\rho)^{0.30}$$

while a dimensional equation gives a good correlation coefficient squared of 0.88

$$\theta = 640\, V^{0.23}\mu_b^{0.20}\rho_t^{0.14}\sigma^{0.25}(\Delta\rho)^{-0.40}$$

where b refers to the bottom coating liquid and t refers to the top fluid, usually air. A much better correlation with a correlation coefficient of 0.99 is obtained for the maximum coating speed at the point of air entrainment:

$$N_{Ca,180} = 0.00019(\mu_b/\mu_t)^{0.33}(\rho_b/\rho_t)^{0.74}$$

The dimensional equation with the same correlation coefficient is

$$V_{180} = 180\mu_b^{-0.67}\mu_t^{0.33}\rho_t^{-0.84}$$

With air as the upper fluid, a dimensional correlation ($r^2 = 0.95$) is

$$V_{180} = 5.11\mu_b^{-0.67}$$

which is the same viscosity dependency as found by Burley and Kennedy.

The poorer correlation of the equation for the dynamic contact angle compared to that for the entrainment velocity may mean that this is not the correct form of the equation. The poorer correlation of the dimensionless equations, compared to the dimensional equations, may be caused by the omission of a significant group due to our inability to find a readily accessible characteristic length.

The surface tension to be used in these equations is the dynamic surface tension, for adding surfactant to an aqueous solution does not affect the contact angle. At high base velocities, the age of the fresh surface formed near the plunge point is so short that the surface tension is still that of pure liquid. The correlation shows that higher entrainment velocities can be obtained by lowering the fluid viscosity at the contact line.

INTRODUCTION

In many coating processes the coating solution passes through an air gap onto the moving base. The ability to get a good coating depends on the ability of the coating solution to wet the base. This, in turn, is related to the contact angle that the coating solution makes with the base. It is the purpose of this study to investigate some of the factors, including the velocity of the base, that affect the dynamic contact angle.

It is well known that advancing contact angles are higher than equilibrium values. Most of the older studies have reported on very low velocities of advancement that are much lower than coating speeds. A 1964 review by Elliott and Riddiford goes over the older work.

Schwartz and Tejada (1972) reviewed the more recent literature and compared theoretical work on plastics and metals, at velocities up to 0.3 m/s. At the lowest velocities they found a region where the contact angle is the static angle. Above this region the Blake-Haynes (1966) model holds. This involves a hyperbolic sine function, and was tested by Blake and Haynes at velocities under 0.01 m/s. At higher velocities the Friz (1965) model

$$\tan\theta = 3.4\, N_{Ca}^{1/3} \qquad (1)$$

is followed, where N_{Ca} is the capillary number, $\mu V/\sigma$. Because of the nature of the tangent function, this equation breaks down as the angle approaches 90° It was derived for a slug of fluid being forced through a tube.

Rillaerts and Joos (1980) studied contact angles in flow through a pre-wet capillary. Their theory and data agree that $\cos\theta$-$\cos\theta_s$ should be proportional to the square root of the capillary number and independent of the capillary radius.

Inverarity (1969) examined the dynamic contact angle as a fiber entered a pool of liquid. He found that in some cases the dynamic contact angle is remarkably constant until a certain velocity (0.01 m/s in one system) is exceeded. Above this velocity the contact angle increases rapidly. With solutions or liquids of constant surface tension, the contact angle is a function only of μV, the product of viscosity and velocity. With different surface tensions the curves are different, but tend into one curve at higher contact angles, above 90°. Inverarity concluded that the surface properties play a major role in the dynamic contact angle at low velocities, but a higher velocities the hydrodynamics are controlling.

Deryagin and Levi (1964) were the first to note that with increasing velocities the dynamic contact angle increases to 180°, at which point the air film carried along by the moving base causes incomplete wetting.

Perry (1966) studied dynamic contact angles of a flexible tape entering a pool of liquid, and of a curtain coating onto a horizontal base. He also found a steady increase in contact angle with velocity to 180°, at which point air is entrained. He was able to correlate $N_{We}/(\cos\theta_s - \cos\theta)$ with the Reynolds number, where N_{We} is the Weber number, $\rho LV^2/\sigma$. On both the Weber and the Reynolds numbers the characteristic length, L, is the distance between the static and the dynamic contact lines and is unknown beforehand. Perry found that the velocity of entrainment is increased when the static contact angle is reduced, when the viscosity is reduced, and when the surface tension is increased. The cause of the increase in dynamic contact angle with velocity is the air film carried along by the moving solid, which pushes against the contact line. The maximum velocity attainable before entrainment begins can be increased by applying force to counteract the air film. Perry (1966) did this by putting an object in the liquid pool near the base, and also by blowing air against the bead in the curtain coater. Beguin (1954) earlier had used a pressure differential across the bead in a coater to increase coating speeds.

Burley and Kennedy (1976a,b, 1978; also Kennedy and Burley, 1977) studied the dynamic contact angles, the shape of the meniscus, and the velocity of air entrainment for a polyester tape plunging into a number of liquids. They noted (1976a) that the velocity of air entrainment is independent of tape surface for several different polyester tapes, although their data show slight differences. Using the depression of the surface to the plunge point as a characteristic length, Burley and Kennedy (1976a, 1976b, 1977) correlated the velocity of air entrainment as

$$N_{We} = 0.834\, N_{Re}^{0.80} \qquad (2)$$

where N_{Re} is the Reynolds number, $L\rho V/\mu$. Perry's data (1966), when presented in this form, is

TABLE 1. FLUID PROPERTIES, STATIC CONTACT ANGLES, AND AIR ENTRAINMENT VELOCITIES[a]

Fluid	Density kg/m³	Viscosity mPa·s	Surface Tension mN/m	θ_s degrees	V_{180} m/s
Water	1000	0.94	72	32	4.6–6.8
Water + Aerosol OT[a]	1000	0.94	41	38	
70% Glycerine	1180	17	63	35	0.83
70% Glycerine + Aerosol OT[a]	1180	18	53	39	0.92
85% Glycerine	1220	93	63	44	0.4
85% Glycerine + Aerosol OT[a]	1220	84	54	47	0.4
99% Glycerine	1260	993	63		0.076
1.05% Sodium Cellulose Sulfate[a]	1000	49	69	44	3–6
1.26% Sodium Cellulose Sulfate[a]	1000	101	69	42	
Mineral Oil	880	174	32	53	0.10
Castor Oil	969	960	35	65	0.044
Corn Oil	923	59	34	68	0.24
Kerosene	819	1.8	24		4.6
Isopropanol	785	2.3	22	31	3.3
2.7% Polyvinyl Alcohol[a]	1010	20	57	34	4.0
2.7% Polyvinyl Alcohol + Aerosol OT[a]	1010	19	47	36	3.3
4.6% Polyvinyl Alcohol[a]	1010	115	59	33	2.5
4.6% Polyvinyl Alcohol + Aerosol OT[a]	1010	115	49	38	2.4
Air	1.207	0.0183			

[a] Liquids containing polymers or surfactant were not used in the data analyses.

TABLE 2. DATA FOR TWO-FLUID RUNS

Upper Fluid	Lower Fluid	ρ_t kg/m³	ρ_b kg/m³	μ_t mPa·s	μ_b mPa·s	σ_i mN/m	θ_s deg	V_{180} m/s
Mineral Oil	Water	880	1000	174	0.94	55	68	0.00087
Castor Oil	Water	969	1000	960	0.94	26	74	0.00091
Corn Oil	Water	923	1000	59	0.94	27	71	0.00017
Kerosene	Water	819	1000	1.8	0.94	33	66	0.0055
Mineral Oil	1.26% SCS	880	1000	174	105	31	60	0.0011
Castor Oil	1.26% SCS	969	1000	960	98	19	73	0.0013
Corn Oil	1.26% SCS	923	1000	59	98	23	54	0.0013
Kerosene	1.26% SCS	819	1000	1.8	105	30	60	0.0037

$$N_{We} = 0.196\, N_{Re}^{0.83} \tag{3}$$

The depression of the surface to the plunge point is, of course, not known beforehand. Burley and Kennedy (1976b, 1977) were able to obtain an equally good correlation with

$$V_{180} = 67.7 \left[\mu \left(\frac{g}{\rho\sigma}\right)^{0.5}\right]^{-0.67} \tag{4}$$

They found that with viscosities above 462 mPa·s the air entrainment velocity is constant at 0.095 m/s (1977).

Burley and Kennedy (1976b) also found, using liquids of constant viscosity but different surface tensions, that the dynamic contact angle at a given tape velocity decreased with increasing surface tension. This was for dynamic contact angles above 125°. In contrast to Perry (1966) they found that the static contact angle had no effect on the air entrainment velocity.

A plot of cos θ versus the capillary number, $\mu V/\sigma$, for three different glycerin-water solutions (Burley and Kennedy, 1976b) gave three different curves, not one as suggested by Inverarity (1969), but Inverarity's data fall in the same region. The capillary number for air entrainment varied from 0.2 to 0.8 for all the systems they studied, as compared to Wilkinson's (1975) results where, using a pre wet cylinder, air entrainment occurs at a capillary number of 1.2.

Kennedy and Burley (1977, also Burley and Kennedy, 1978) developed a theory which predicts quite well the shape of the meniscus when a tape plunges vertically into a pool of liquid. Here too, however, they require the depth of depression of the surface, and this length is not known beforehand.

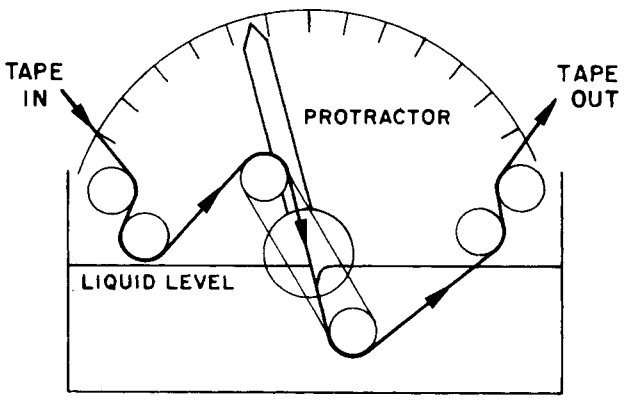

Figure 1. Sketch of apparatus.

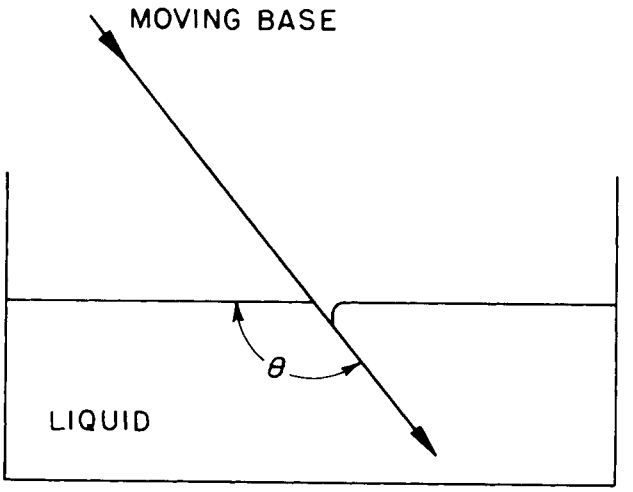

Figure 2. Measurement of contact angle.

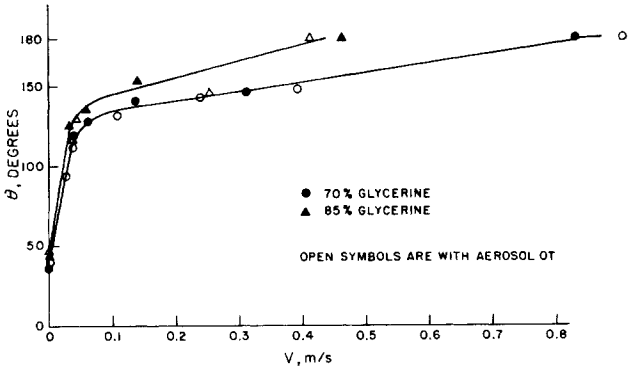

Figure 3. Contact angle vs. tape velocity.

Blake and Ruschak (1979) found that there is an extended velocity region where the contact angle remains at 180° but air is still not entrained. Upon further increase in tape velocity the wetting line breaks into two or more inclined segments, such that the forward component of velocity remains constant. In one case, the 180° angle occurred at a plunging tape velocity of 19.4 cm/s, while air was not entrained until 25 cm/s.

Bolton and Middleman (1980) studied air entrainment velocities using a pre-wet rotating cylinder, similar to the experiments of Wilkinson (1975). They found, both experimentally and theoretically, that the capillary number ($\mu V/\sigma$) at air entrainment should be a function only of a physical properties number, which Fulford (1964) wrote as $g\mu^4/\rho\sigma^3$. Except for the high viscosity region ($N_{pp} \gg 0.13$) their data can be represented as

$$N_{Ca} = 3.4\, N_{pp}^{0.2} \tag{5}$$

DIMENSIONAL ANALYSIS

The dynamic contact angle should be related to the various forces acting on the system. With a given film base, the surface properties of the base should not enter into the relation. Acting on the system are gravity, inertial, surface, and viscous forces. Per unit mass of liquid, the forces have dimensions of acceleration, L/T^2, and are:

a. Gravity: $F_{gr} = g$

b. Inertial: F_{in} = rate of change of momentum
$F_{in} = mV/mT = (mV/m)\,(V/L) = V^2/L$

c. Surface: $F_{sur} = \sigma L/\rho L^3 = \sigma/\rho L^2$

d. Viscous: $F_{vis} = A\tau/\rho L^3 = (L^2/\rho L^3)(\mu du/dy)$
$= (\mu/\rho L)(V/L) = \mu V/\rho L^2$

From these four forces we can get three independent ratios of forces, giving three well-known dimensionless groups:

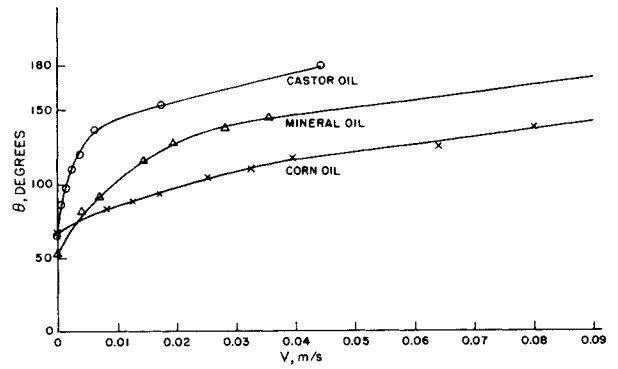

Figure 4. Contact angle vs. tape velocity.

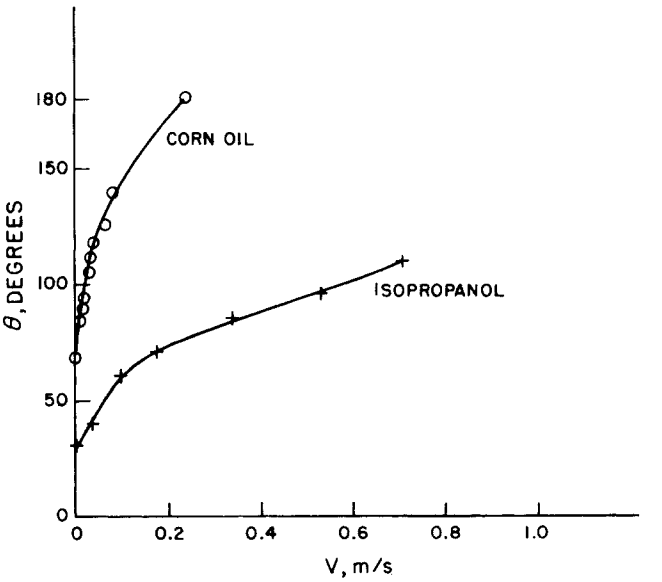

Figure 5. Contact angle vs. tape velocity.

a. Reynolds No. $= N_{Re} = F_{in}/F_{vis}$
$= (V^2/L)/(\mu V/\rho L^2) = LV\rho/\mu$

b. Froude No. $= N_{Fr} = F_{in}/F_{gr}$
$= (V^2/L)/g = V^2/Lg$

c. Weber No. $= N_{We} = F_{in}/F_{sur}$
$= (V^2/L)/(\sigma/\rho L^2) = \rho LV^2/\sigma$

However, we do not have an accessible characteristic length. If we use one group, say N_{Re}, to eliminate the characteristic length, we end up with two independent groups. The ones we have chosen are the capillary number, and a physical properties number (Fulford, 1964) which does not involve velocity.

$$\text{Capillary No.} = N_{Ca} = \frac{F_{vis}}{F_{sur}} = \frac{N_{We}}{N_{Re}} = \frac{\mu V}{\sigma} \cdot \tag{6}$$

$$\text{Physical Properties No.} = N_{pp} = \frac{F_{gr} F_{vis}^4}{F_{in}^3 F_{sur}^2} = \frac{N_{We}^3}{N_{Re}^4 N_{Fr}} = \frac{g^4 u}{\rho\sigma^3} \tag{7}$$

Other dimensionless groups could involve ratios of the properties of the upper fluid (usually air) to that of the lower fluid. Thus, we might expect that the dynamic contact angle might be

$$\theta = f\left(N_{Ca}, N_{pp}, \frac{\mu_t}{\mu_b}, \frac{\rho_t}{\rho_b}, \frac{\rho_b - \rho_t}{\rho_b}\right) \tag{8}$$

More specifically we would hope the relationship would be of the form

$$\theta = kN_{Ca}^a N_{pp}^b \left(\frac{\mu_t}{\mu_b}\right)^c \left(\frac{\rho_t}{\rho_b}\right)^d \left(\frac{\rho_b - \rho_t}{\rho_b}\right)^e \tag{9}$$

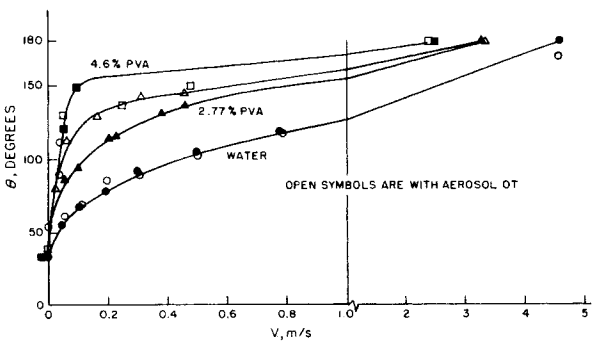

Figure 6. Contact angle vs. tape velocity.

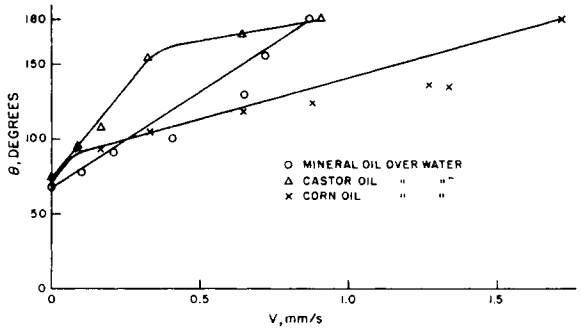

Figure 7. Contact angle vs. tape velocity.

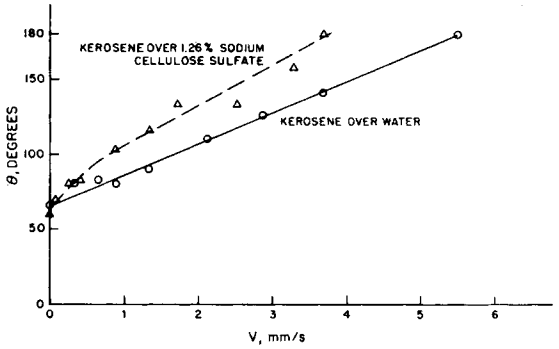

Figure 9. Contact angle vs. tape velocity.

As, at very low velocities, the contact angle would equal θ_s, the static contact angle, the equation might be

$$\theta - \theta_s = kN_{Ca}^{a}N_{pp}^{b}\left(\frac{\mu_t}{\mu_b}\right)^{c}\left(\frac{\rho_b}{\rho_c}\right)^{d}\left(\frac{\rho_b - \rho_t}{\rho_b}\right)^{e} \tag{10}$$

The air entrainment velocity could then be found from the capillary number at which the contact angle is 180°, or, we would hope,

$$N_{Ca,180} = kN_{pp}^{a}\left(\frac{\mu_t}{\mu_b}\right)^{b}\left(\frac{\rho_t}{\rho_b}\right)^{c}\left(\frac{\rho_b - \rho_t}{\rho_b}\right)^{d} \tag{11}$$

We would not expect the static contact angle to be very important here, relative to the 180° dynamic angle.

EXPERIMENTAL

We measured the dynamic contact angle of a number of solutions as a function of the velocity of a 16 mm wide, gelatin-coated polyester tape entering a pool of liquid. In some cases the tape plunged through the interface between two immiscible liquids; that is, the upper fluid was an oil rather than air. The solutions and their properties are given in Tables 1 and 2. All measurements were done at room temperature, approximately 23°C. Viscosities were measured in Cannon-Fenske capillary viscometers, and surface tensions with a deNoüy ring tensiometer. The drop weight method (Adamson, 1967) was used to measure interfacial tensions. Densities were measured with a hydrometer.

Fowkes and Harkins (1940) recommended the tilting plate method as best for accurate measurements of static contact angles, with the axis of rotation lying in the solid-liquid intersection. We used the apparatus illustrated in Figure 1 in order to be able to alter the angle at which the tape entered the solution. The container was made from 1/4 in. (6.4 mm) polymethyl methacrylate (Lucite). Its external dimensions are 155 mm long, 68 mm wide, and 75 mm high. The base extends forward 3 cm, so that the unit can be screwed down to a wooden base holding the drive and tape reel assembly. The normal liquid depth is about 43 mm. The 16 mm tape enters from a 90 mm diameter reel, and is taken up on a similar reel driven through a chain drive by one of three d.c. gear motors with controllers. Tape speeds, from 0.0002 to 7 m/s, are found by measuring the rotation rate of the take-up reel with a tachometer, and also the diameter of the tape on the reel. A scraper removes much of the liquid ahead of the take-up reel. The 8 mm diameter central nylon guides, with flanges, are fixed 50 mm apart on a 12 mm wide stainless steel plate. This plate is mounted on a shaft extending through the rear wall, using an O-ring seal. The pointer is mounted externally on the same shaft. The transparent plastic protractor is attached to the outside of the rear wall. To determine the contact angle, at any tape velocity, we tilt the tape by rotating the pointer until the liquid surface is flat right up to the tape as shown in Figure 2. The contact angle is then read off the protractor. The apparatus worked best for angles between 45° and 135°. For air entrainment velocities, the pointer is adjusted so that the tape enters vertically and the speed is increased until air is entrained into the pool of liquid. Within the precision of measurement, about 1 or 2°, the dynamic contact angle measured by tilting the tape is equal to that measured by photographing the profile as the tape enters vertically, and measuring the angle on the photograph. Tables 1 and 2 include the static contact angles and the air entrainment velocities, listed as V_{180}. Plots of contact angle versus tape velocity are shown in Figures 3–9.

DISCUSSION

We see in Figures 3–9 that the dynamic contact angle increases with tape velocity from its static value until it reaches 180°, the upper fluid entrainment velocity. In some cases, as for the tape plunging into a 1.26% sodium cellulose sulfate solution with mineral oil or kerosene floating on it (Figures 8 and 9) there is a linear relationship between contact angle and tape velocity; in most cases the relationship is non-linear. However, linear relations can be obtained (except at the low tape velocities) by plotting the log of the contact angle against the log of the tape velocity, expressed as the capillary number of the lower fluid, $\mu_b V/\sigma$. For the Newtonian fluids with air as the upper fluid this is shown in Figure 10. Obviously, at low tape velocities the line must become horizontal and equal to the static contact angle.

In the two-fluid cases we defined this horizontal portion and the bend in the line, and were able to get a linear plot by subtracting the static contact angle from the dynamic angle, as in Figure 11.

Also, as mentioned earlier, Blake and Ruschak (1979) found that the contact angle remains at 180° over a range of velocities before air is entrained. Thus there is some uncertainty about the location of the points on the velocity axis, found by visible entrainment but plotted as 180°. In an example given by Blake and Rushak (1979), this uncertainty was about 25%. In other words, our 180° points should be displaced slightly to the left. This would not greatly affect the logarithmic plots.

In Figure 10 we see, with air as the upper fluid, that all the lines for the different Newtonian liquids fall relatively close, within one

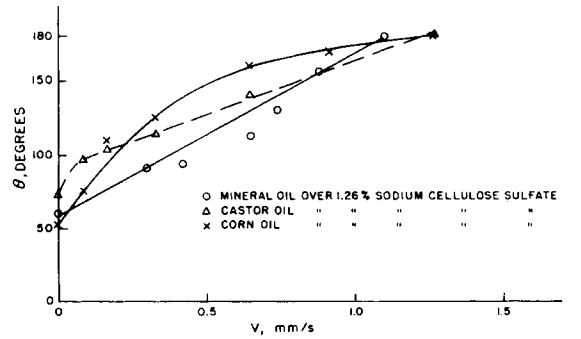

Figure 8. Contact angle vs. tape velocity.

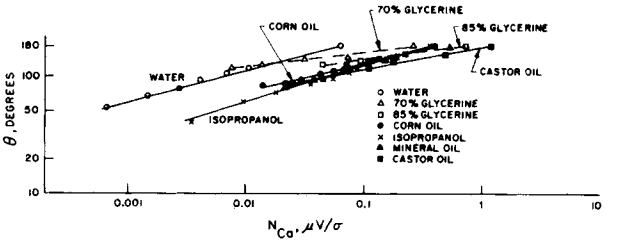

Figure 10. Contact angle vs. capillary number.

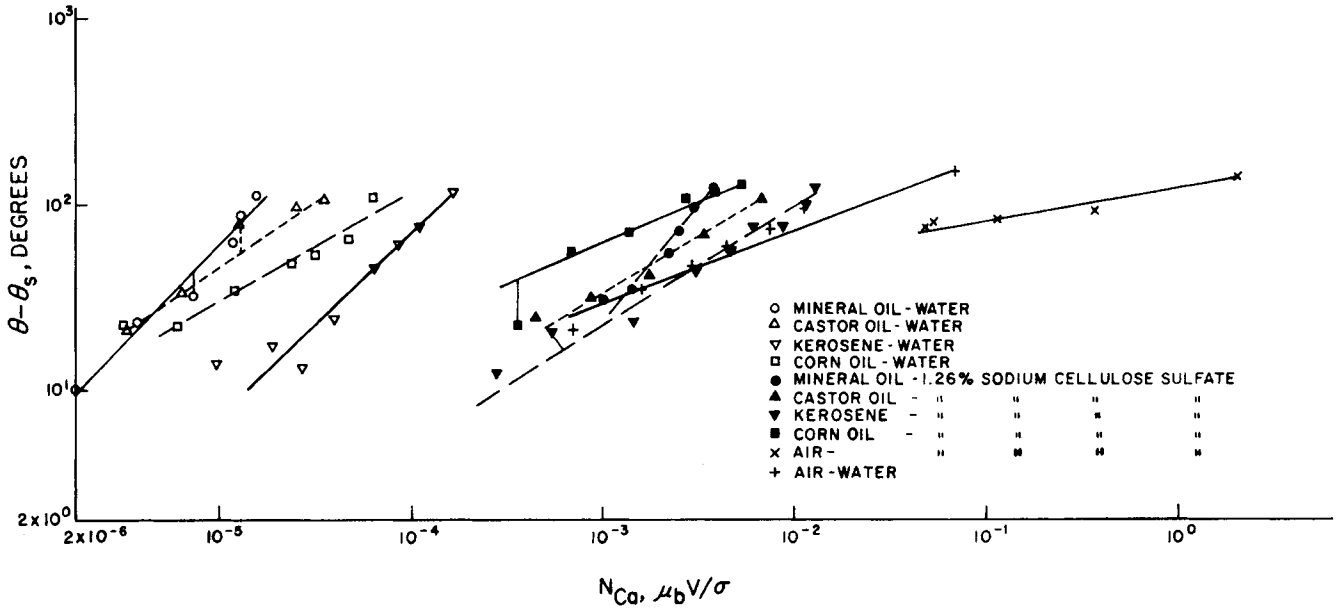

Figure 11. Dynamic minus static contact angle vs. capillary number.

decade in capillary numbers, of one to the other. However, as the lines do differ, we see that more variables than just the capillary number are needed to define the contact angle, in contrast to the results of Rillaerts and Joos (1980) on contact angles in a capillary. With immiscible oils as the upper fluid the lines span many decades, as shown in Figure 11. Thus the properties of the upper fluid are extremely important.

Some data were taken with Aerosol OT in the aqueous solutions. Aerosol OT, in spite of lowering the surface tension (Table 1), had no effect on the dynamic contact angle in the case of glycerin solutions (Figure 3) or water (Figure 6), but did have an effect with polyvinyl alcohol solutions (Figure 6). The work of Dyba and Miller (1970) implies that the dynamic surface tension should be considered. They found that with increasing concentrations of sodium dodecyl sulfate in water—even well above the critical micelle concentration at which the static surface tension remains unchanged—the velocity of a filament needed to give a dynamic contact angle was 90° kept increasing. We suggest that, at the high tape velocities and therefore very young ages of the surface near the contact point, the dynamic surface tension is near that of the surfactant-free material.

Although we have included some polymeric solutions (polyvinyl alcohol and sodium cellulose sulfate) for completeness, we have used only the results for the Newtonian liquids in our analyses. We do not know how to calculate the proper viscosity for shear thinning fluids, and we do not know how to include the viscoelastic properties of polymeric solutions.

REGRESSION ANALYSIS

We did a regression analysis on the data according to the dimensionless Eqs. 9, 10, and 11, and also with the dimensional variables. If more than one variable was insignificant by the "t" test, the least significant variable was dropped. This was continued until all the variables were highly significant, that is, significant at the 99% level. We used the DISTAT package of the Computer Sciences Corporation time sharing service.

The results of the regression analysis are given in Table 3. First of all, Table 3 shows that the regression equations involving θ-θ_s have a poorer correlation (lower r^2) than do the equations not involving θ_s, the static contact angle. Thus, in Table 3, compare the r^2 values for Eqs. A3 (0.68) and A4 (0.83) with Eq. A1 (0.90), and Eq. A2 (0.90) or B3 (0.76) and B4 (0.81) with B1 (0.70) and B2 (0.88). The poorer correlation may only indicate that the form of the equation involving the static contact angle is not correct; thus, in place of θ-θ perhaps we should use cos θ-cos θ_s, or perhaps the equation is no longer a simple power relationship.

The dimensional Eqs. A2, A4, B2, and B4 in Table 3 indicate that the dynamic contact angle increases with tape velocity, bottom fluid viscosity, surface or interfacial tension, top fluid density, and, by B2, by a decrease in the difference in density of the two fluids.

It is easy to show that the dimensionless equation for the contact angle with air as the upper fluid, Eq. A1, is essentially identical to the dimensional form Eq. A2, and the r^2 values are the same for

TABLE 3. REGRESSION EQUATIONS FOR DYNAMIC CONTACT ANGLES AND AIR ENTRAINMENT VELOCITIES

	A. With Air As Top Fluid	r^2	B. All Data	r^2
1.	$\theta = 6.24 N_{Ca}^{0.22} N_{PP}^{-0.099} \left(\frac{\mu_b}{\mu_t}\right)^{0.36}$	0.90	$\theta = 402 N_{Ca}^{0.20} N_{PP}^{-0.0096} \left(\frac{\rho_t}{\rho_b}\right)^{0.11} \left(\frac{\rho_b}{\Delta\rho}\right)^{0.30}$	0.70
2.	$\theta = 73 V^{0.22} \mu_b^{0.18} \sigma^{0.11}$ $\theta = 110 V^{0.22} \mu_b^{0.18}$	0.90 0.88	$\theta = 640 V^{0.23} \mu_b^{0.20} \rho_t^{0.14} \sigma^{0.25} (\Delta\rho)^{-0.40}$	0.88
3.	θ-$\theta_s = 901 N_{Ca}^{0.20} \left(\frac{\rho_t}{\rho_b}\right)^{0.16} \left(\frac{\mu_t}{\mu_b}\right)^{0.050}$	0.68	θ-$\theta_s = 128 N_{Ca}^{0.37} N_{PP}^{-0.042} \left(\frac{\rho_b}{\Delta\rho}\right)^{0.84}$	0.67
4.	θ-$\theta_s = 27.4 V^{0.41} \mu_b^{0.26} \sigma^{0.27}$	0.83	θ-$\theta_s = 2910 V^{0.47} \mu_b^{0.32} \rho_t^{0.16} \sigma^{0.53} (\Delta\rho)^{-0.83}$	0.81
5.	$N_{Ca,180} = 0.767 N_{PP}^{0.088}$	0.85	$N_{Ca,180} = 0.00019 \left(\frac{\mu_b}{\mu_t}\right)^{0.33} \left(\frac{\rho_b}{\rho_t}\right)^{0.74}$	0.99
6.	$V_{180} = 5.11 \mu_b^{-0.67}$	0.95	$V_{180} = 1.80 \mu_b^{-0.67} \mu_t^{-0.30} \rho_t^{-0.84}$	0.99

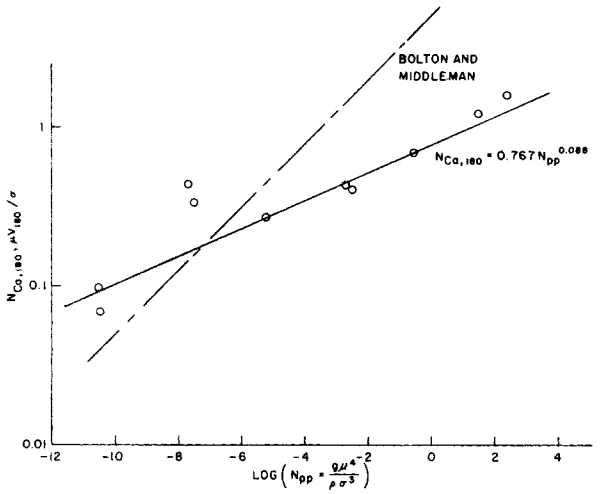

Figure 12. Capillary number at air entrainment vs. physical properties number.

both. Including the two fluid data, we can show that the dimensionless Eq. B1 has a different sign in the surface tension dependency compared to the dimensional Eq. B2. The square of the correlation coefficient is only 0.70 for Eq. B1 compared to 0.88 for the dimensional equation.

We do not know why the dimensionless equation should be so much poorer, unless we have omitted a variable. As we showed in our dimensional analysis, we have left out one variable because of our inability to get a characteristic length. The depression of the surface we do not know beforehand. Perhaps the rise of the meniscus to the static contact point might serve as a characteristic length.

It is also possible that the 16 mm wide tape is not wide enough to eliminate edge effects, and also that electrostatic effects play a role, especially with the non-conductive liquids.

Equation 8, from Rillaerts and Joos (1980), does not hold, for a plot of cos θ-cos θ_s against capillary number shows much scatter.

UPPER FLUID ENTRAINMENT VELOCITIES

Table 3 shows that the correlation for upper fluid entrainment velocities are quite good, with squares of the correlation coefficients ranging from 0.85 to 0.99. Equation A5, with air as the upper fluid,

$$N_{Ca,180} = 0.767\,N_{pp}^{0.088} \quad r^2 = 0.85 \tag{A5}$$

is similar in form to Eq. 5

$$N_{Ca,180} = 3.4\,N_{pp}^{0.2} \tag{5}$$

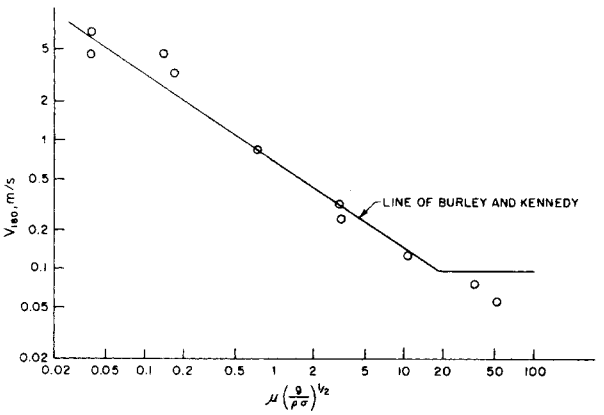

Figure 13. Air entrainment velocities plotted according to the correlation of Burley and Kennedy.

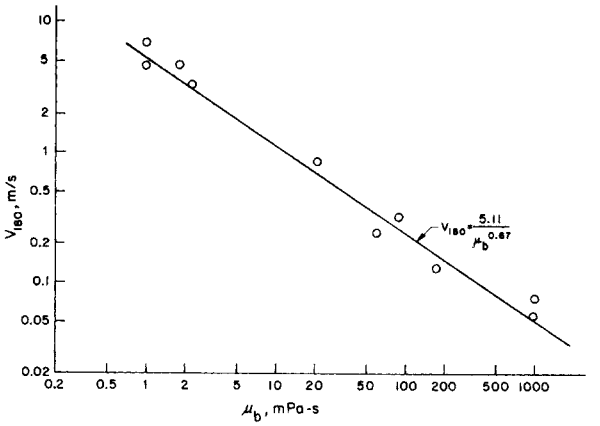

Figure 14. Air entrainment velocities as a function of viscosity.

which Bolton and Middleman (1980) found with a rotating cylinder. Figure 12 is a log-log plot of the capillary numbers at air entrainment versus the physical properties numbers. The data fit equation A5 fairly well, but do not fit Eq. 5. Of course, a pre-wet rotating cylinder is not the same as a plunging tape with its own unique surface.

Burley and Kennedy (1976b, 1977) correlated their plunging tape data with

$$V_{180} = 67.7\left[\mu\left(\frac{g}{\rho\sigma}\right)^{0.5}\right]^{-0.67} \tag{4}$$

Our data fit this relationship quite well, as shown by Figure 13. However, Burley and Kennedy found that the air entrainment velocities did not drop below 0.095 m/s. We did not find a lower limit.

The viscosity dependency in Eq. 6 is identical to our dimensional correlation A6 with air as the top fluid.

$$V_{180} = 5.11\,\mu_b^{-0.67} \quad r^2 = 0.95 \tag{A6}$$

We found that no other variables were significant. Equation A6 is plotted along with the data in Figure 14. As indicated by the high, 0.95 value of the square of the correlation coefficient, the correlation is very good, and considerably better than the dimensionless correlation, Eq. A5. Equation A5 shows almost the same viscosity dependency as A6, but includes a density and a surface tension dependency, which, from the data, not only are not significant but reduce the value of the correlation coefficient. The lack of surface tension dependency was anticipated by Inverarity (1969) who pointed out that at higher velocities the hydrodynamics, and not the surface forces, are controlling.

The poorer correlation of the dimensionless Equation A6 as compared to the dimensional Equation A5 may be explained, as in the discussion on the contact angle correlations, by our lack of ready access to a characteristic length and the consequent loss of one dimensionless group.

With all the data on upper fluid entrainment velocities included, the dimensionless and dimensional equations are Eqs. B5 and B6 in Table 3. From Eq. B6 we see that the upper fluid entrainment velocity is increased by reducing the viscosities of both upper and lower fluids and also the upper-fluid density. Therefore a gas (air) is desirable as the upper fluid for highest upper fluid entrainment velocities. The lower-fluid density did not vary enough to cause significant effects. However, we would expect that, because of buoyancy effects, just as a low upper-fluid density is desirable for high entrainment velocities, so too would a high lower-fluid density be desirable. The ratio of the two densities should be important, as indicated in Eq. B5. As in Eq. A5, surface (or interfacial) tension appears in the dimensionless equations, but it does not seem to be important.

It is instructive to set the contact angle at 180 degrees in Eqs. A1, A2, B1 and B2, and compare the results to Eqs. A5, A6, B5 and B6.

We see significant differences between the pairs. As noted earlier, the correlation coefficient for the equations relating upper fluid entrainment velocities are much higher than for the equations relating dynamic contact angles. We therefore would expect greater errors when using the contact angle equations to predict entrainment velocities, setting the contact angle at 180°.

CONCLUSIONS

For a gelatin-subbed polyester tape plunging into a pool of liquid, we have correlated dynamic contact angles and upper fluid entrainment velocities with fluid properties and tape velocities. The dimensional correlations are better than the dimensionless correlations, perhaps due to our inability to determine a suitable characteristic length. The correlations for the entrainment velocities were considerably better than for the contact angles. With air as the upper fluid, the air entrainment velocity is proportional to the viscosity to the −0.67 power. No other variables were significant. The viscosity dependency is the same as found by Burley and Kennedy.

NOTATION

a,b,c,d,e = slopes or exponents in experimental equations
F_{gr} = gravitational or buoyancy force per unit mass, m/s^2
F_{in} = inertial force per unit mass, m/s^2
F_{sur} = surface force per unit mass, m/s^2
F_{vis} = viscous force per unit mass, m/s^2
g = acceleration of gravity, 9.807 m/s^2
k = intercept in experimental equations, degrees or m/s
L = length, m
N_{Ca} = capillary Number, $\mu_b V/\sigma$, dimensionless
N_{Fr} = Froude number, V^2/Lg, dimensionless
N_{pp} = physical properties group, $g\mu_b^4/(\rho_b\sigma^3)$, dimensionless
N_{Re} = Reynolds number, $LV\rho/\mu$, dimensionless
N_{We} = Weber number, $\rho LV^2/\sigma$, dimensionless
r = correlation coefficient
t = time, s
V = velocity, m/s
μ = dynamic viscosity, mPa·s
ρ = density, kg/m^3
σ = surface tension, mN/m
θ = dynamic contact angle, degrees
θ_s = equilibrium static contact angle, degrees

Subscripts

b = bottom layer
t = top layer
180 = point of entrainment, where the contact angle is 180°

LITERATURE CITED

Adamson, A. W., "The Physical Chemistry of Surfaces," 2nd ed., 21, Interscience, New York (1967).
Beguin, A. E., Method of Coating Strip Material, U.S. Patent 2,681,294 (1954).
Blake, T. D., and J. M. Haynes, "Kinetics of Liquid-Liquid Displacement," *J. Colloid Interface Sci.*, **30**, 421 (1969).
Blake, T. D., and K. J. Ruschak, "A Maximum Speed of Wetting," *Nature*, **282**, 489 (1979).
Bolton, B., and S. Middleman, "Air Entrainment in a Roll Coating System," *Chem. Eng. Sci.*, **35**, 597 (1980).
Burley, R., and B. S. Kennedy, "A Study of Dynamic Wetting Behavior of Polyester Tapes," *Br. Polymer J.*, **8**, 140 (Dec., 1976a).
Burley, R., and B. S. Kennedy, "An Experimental Study of Air Entrainment at a Solid-Liquid-Gas Interface," *Chem. Eng. Sci.*, **31**, 901 (1976b).
Burley, R., and B. S. Kennedy, "Dynamic Wetting and Air Entrainment at a Liquid-Solid-Gas Junction," Chapt. 15, J. F. Padday, ed., *Wetting, Spreading, and Adhesion*, 327, Academic Press, London (1978).
Deryagin, B. M., and S. M. Levi, "Film Coating Theory," (translation of the 1959 Russian Edition, "The Physical Chemistry of Coating Thin Layers on a Moving Support), 137, Focal Press, London (1964).
Dyba, R. V., and B. Miller, "Dynamic Measurements of the Wetting of Single Filaments," *Textile Res. J.*, **40**, 884 (1970).
Elliott, G. E. P., and A. C. Riddiford, "Contact Angles," *Recent Progress in Surface Science*, **II**, J. F. Danielli, K. G. A. Pankhurst, and A. C. Riddiford, eds., 111, Academic Press, New York (1964).
Fowkes, F. M., and W. D. Harkins, "The State of Monolayers Adsorbed at the Interface Solid-Aqueous Solution," *J. Am. Chem. Soc.*, **62**, 3377 (1940).
Friz, G., "On the Dynamic Contact Angle in the Case of Complete Wetting," *Z. Angew. Phys.*, **19** (4), 374 (1965).
Fulford, G. D., "The Flow of Liquids in Thin Films," T. B. Drew et al., eds., *Advances in Chem. Eng.*, **5**, 151, Academic Press, New York (1964).
Inverarity, G., "Dynamic Wetting of Glass Fibre and Polymer Fibre," *Brit. Polymer J.*, **1**, 245 (1969).
Kennedy, B. S., and R. Burley, "Dynamic Fluid Interface Displacement and Prediction of Air Entrainment," *J. Colloid Interface Sci.*, **62**, 48 (1977).
Perry, R. T., "Fluid Mechanics of Entrainment Through Liquid-Liquid and Liquid-Solid Junctions," Ph.D. Thesis, Chem. Eng., U. of Michigan, 1966; University Microfilms, 76-14, 639 (1967).
Rillaerts, E., and P. Joos, "The Dynamic Contact Angle," *Chem. Eng. Sci.*, **35**, 883 (1980).
Schwartz, A. M., and S. B. Tejada, "Studies of Dynamic Contact Angles on Solids," *J. Colloid Interface Sci.*, **38**, 359 (1972).
Wilkinson, W. L., "Entrainment of Air by a Solid Surface Entering a Liquid/Air Interface," *Chem. Eng. Sci.*, **30**, 1227 (1975).

Manuscript received February 9, 1981; revision received June 10, and accepted July 14, 1981.